Effect of Microalloying with Ti on the Corrosion Behaviour of Low Carbon Steel in a 3.5 wt.% NaCl Solution Saturated with CO$_2$

Ali R. Sheikh (iD)

AGH University of Science and Technology, Kraków, Poland
* Corresponding author: E-mail: ars405@gmail.com

Abstract

A problem is defined to investigate the effect of titanium traces on the corrosion behaviour of low carbon steel. In theory titanium effects surface properties like abrasion resistance in medium carbon steels and corrosion resistance in low as well as medium carbon steels. The present research as indicated by the topic is aimed to experimentally mark the effect of titanium traces on corrosion resistance in the available low carbon steel specimens.

The effect of microalloying with titanium (i.e.0.02wt.%) on the corrosion behavior of low carbon steel in a 3.5 wt.% NaCl solution was studied by electrochemical, SEM, and Raman spectroscopy techniques. The electrochemical results showed that the corrosion of the Ti-bearing steel improved by around 30% compared with the Ti-free steel. The titanium microalloying led to the formation of a more compact corrosion product layer on the metal surface. The SEM analysis showed that the Ti-bearing sample had a smoother surface compared with the Ti-free steel.

Keywords: Raman spectroscopy, Carbon dioxide corrosion, Titanium microalloying, Electrochemical experiments

1. Introduction

Low-carbon steels (LCSs) are often used for pipeline applications mainly due to their cost [1-2]. However, given the extreme conditions in the gas/oil reservoirs, LCS corrodes easily. The majority of failures reported in oilfield are due to CO$_2$ corrosion (sweet corrosion) and H$_2$S (sour corrosion) [3]. CO$_2$ is often used to enhance oil and/or gas recovery [4]. CO$_2$ dissolves in the operating fluid forming carbonic acid, which corrodes the LCS substrate. [5]. Many researchers have studied the effect of some factors such as CO$_2$ partial pressure, temperature, immersion time,

and pH on the corrosion resistance of carbon steel [6-9], but the effect of microalloying elements on the corrosion behavior of alloy steels in CO$_2$ environments is rarely described [10-11]. Some elements such as Ti, Al, Cr, etc., when added to the alloy have a strong tendency to stimulate the formation of a uniform passive layer (i.e. passivity promoters) [12] hence, increasing the corrosion resistance of steel. Liu et al. [13] observed that the addition of Ti had a beneficial effect on the corrosion resistance of the low-carbon steel, promoting the formation of a dense and compact corrosions products layer. Yu et al. [1] reported the effect of Ti alloying on the corrosion behavior of the low-carbon steel in a H$_2$S/CO$_2$ environment. The authors observed that the Ti-bearing steel

showed an improvement in corrosion resistance compared to the Ti-free steel, resulting from a more compact corrosion product. However, the corrosion behavior of the low-carbon steel in an environment with the presence of pure H_2S or H_2S/CO_2 is different from that of a pure CO_2 environment [1]. H_2S has a strong influence on the corrosion behaviors of the steel, and also in a minimum amount, it is strongly absorbed on the metal surface so that the surface is rapidly covered by a black layer of iron sulfide (i.e. mackinavite) [14]. The corrosion of the steel in the presence of CO_2 is more complex. The formation of iron carbonate on the metal surface can influence the corrosion resistance of the steel. Moreover, the combination of chlorides-containing fluid and CO_2 increases the corrosion rate by a factor of 16 [5]. Therefore, the understanding of this type of corrosion is important for corrosion engineering in the oil and gas field. Consequently, this study reports the effect of Ti on the corrosion behavior of low-carbon steel in saline-saturated CO_2 environment. In this study, the impact of Ti was assessed via electrochemical experiment such as electrochemical impedance spectroscopy (EIS) and potentiodynamic polarisation (PDP). The microstructure and morphological analysis (i.e. SEM and Raman) before and after the corrosion test were also performed in this study.

2. Experimental methods

2.1. Materials and preparation

Two low-alloy steels with the chemical composition listed in Table 1, named LCS and LCS+Ti, were investigated in this work. The samples were machined into a cylindrical shape and embedded into an epoxide resin, leaving a surface area of 1 cm². Each sample was ground with sandpapers up to a grit size of 1200, degreased by alcohol, and before corrosion tests.

Table 1.
Chemical composition of the tested samples

Element	LCS	LCS+Ti
C	0.127	0.115
Si	0.177	0.146
Mn	1.42	1.32
Ti	0.007	0.017
Cr	0.041	0.039
Ni	0.022	0.023
Fe	Bal.	Bal.

2.2. Electrochemical experiments

The measurements were performed on a Gamry reference 600 potentiostat/galvanostat electrochemical system in a three-electrode cell consisting of a saturated calomel electrode (SCE) as a reference electrode, a platinum foil as a counter electrode (CE), and the tested LCs used as working electrodes. The electrochemical impedance spectroscopy (EIS) experiments were carried out after 24 h of immersion over the frequency range of 10 kHz to 10 mHz and with an amplitude of 10 mV at open circuit potential (OCP).

The increase in corrosion resistance (efficiency, E%) was calculated from the polarization resistance ($R_p = R_f + R_{ct}$) obtained from the fitting process with the following equation [6]:

$$E\% = \frac{R_p^{Ti} - R_p}{R_p^{Ti}} * 100 \qquad (1)$$

where R_p^{Ti} and R_p are the polarization resistance values in the presence and absence of the titanium, respectively. The potentiodynamic polarization (PDP) experiments were carried out after 24 hours of exposure to the tested solution at OCP, with a sweep rate from -0.3 V to 0.3 V versus OCP, and a scan rate of 1 mV s⁻¹. The E% was calculated from the measured corrosion current densities (j_{corr}) values using the following equation [15]:

$$E\% = \frac{j_{corr} - j_{corr}Ti}{j_{corr}} * 100 \qquad (2)$$

where $j_{corr}Ti$ and j_{corr} are the corrosion current densities values in the presence and absence of the titanium, respectively.

$$CR \left(mm \ y^{-1}\right) = \frac{3.27 \times 10^{-3} \ i_{corr} \ E_w}{d} \qquad (3)$$

Where i_{corr} is the corrosion current density; E_w is the equivalent weight of the metal and d is the metal density. 3.27×10^{-3} is the conversion factor.

Each time before a test, the steel was ground and polished up 1 μm, ultrasonically washed in ethanol, rinsed, and dried. The experiments were performed in a 3.5 wt.% NaCl solution saturated with CO_2 at $T = 25 \ °C$.

2.2. Surface analysis

The metal surface of the LCS samples was studied via SEM and Raman spectroscopy analysis after they were exposed for 24 in the tested solution. The SEM analysis was carried out by using a JEOL scanning electron microscope. The Raman measurements were performed by using an InVia Raman Spectrometer Renishaw equipped with a charge-coupled device (CCD) camera and the confocal microscope. The spectra were collected with a spectral resolution of 1 cm⁻¹ and in the 4000-50 cm⁻¹ spectral range in three different pints of the surface [16-17].

3. Results and discussion

3.1. Microstructure

Fig. 1a and b, show the microstructure of LCS and LCS+Ti after etching in Nital solution, respectively. As can be seen, the microstructure of the Ti-bearing steel sample appears much finer than that of the Ti-free steel sample. The result is in agreement with the studies reported in the literature that showed that the Ti element was a good inoculant agent for grain refinement [1, 18]. During the

liquid phase solidification, non-metallic micro inclusion particles are formed [19-20]. The grain refinement is due to the precipitation of TiC particles at the grain boundary, which inhibits the grain growth [1, 21-22].
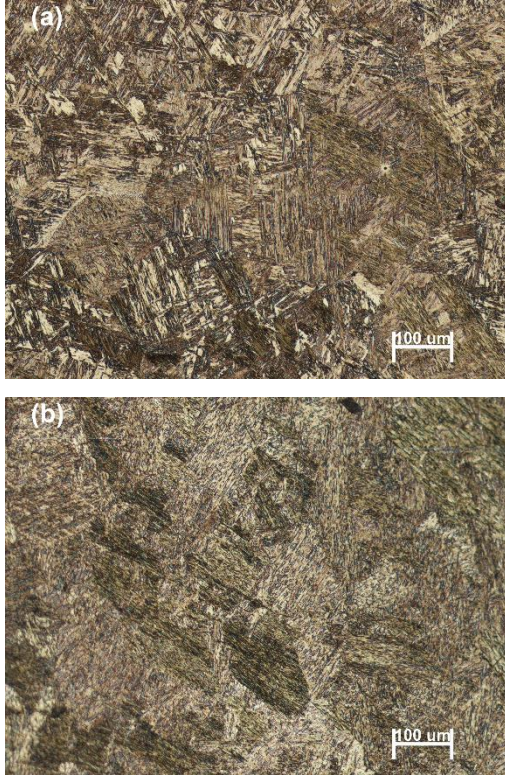
Fig. 1. Optical micrographs of the low carbon steel microstructures. (a) LCS; (b) LCS+Ti

3.2. Electrochemical experiments

Fig. 2a and b, show the EIS measurements performed on the LCs in the tested solution after 24 hours of immersion time. The EIS plots were fitted with the electric equivalent circuit (EEC) shown in Fig. 1a (inset) and the fitting parameter were listed in Table 2. R_s represents the resistance of the solution. R_f and Q_f are the resistance and the capacitance of the film (i.e. corrosion/passive film), respectively. R_{ct} and Q_{dl} are the charge transfer resistance and the capacitance of the double layer, respectively. Due to the imperfection of the metal surface, the double-layer capacitance (C_{dl}) was simulated via a constant phase element (CPE) [6, 15]. The impedance of CPE is described by the following equation:

$$Z_{CPE} = \frac{1}{Q(j\omega)^n} \tag{4}$$

where Q is the CPE constant, n is the exponent, j is the imaginary number and ω is the angular frequency at which Z reaches its maximum value. The parameter n quantifies the imperfections of the surface. For $n = 1$, CPE is a pure capacitor, and for $n = -1$, CPE is an inductor [6, 15]. The data shows that R_p increased in the

presence of Ti micro-inclusion in the metallic matrix from 231.41 to 325.74 Ω cm^2, reflecting an improvement in corrosion resistance of around 30%. Moreover, the steel with Ti has a higher R_f compared to the Ti-free steel, indicating that the trace addition of Ti improved the resistance of the low carbon steel [23]. This improvement may be ascribed to the formation of a denser corrosion layer on the metal surface, as observed from the PDP experiments.
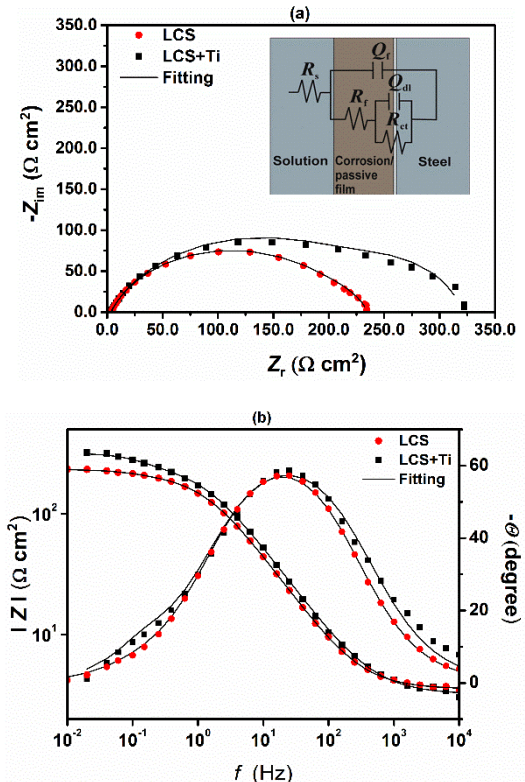
Fig. 2. EIS plot of the steels after 24 hours of immersion in 3.5 wt.% NaCl saturated with CO_2. (a) Nyquist, (b) Bode

Table 2.
EIS parameters

Sample	LCS	LCS+Ti
R_s (Ω cm^2)	3.54	3.20
Q_1 (mΩ^{-1} sn cm^{-2})	0.87	0.77
n	0.79	0.79
R_1 (Ω cm^2)	17.71	54.64
Q_{dl} (mΩ^{-1} sn cm^{-2})	66.93	19.32
n	0.87	0.90
R_{ct} (Ω cm^2)	213.70	271.10
$R_p = R_1 + R_{ct}$ (Ω cm^2)	231.41	325.74
$\chi 2$ (10^{-4})	2.65	20.30

Fig. 3 and Table 3 show the PDP plots and the corrosion kinetic parameters of the steels with and without the presence of Ti after 24 hours of immersion in the tested solution, respectively. As can be seen from the data, the addition of Ti leads to a decrease of a few orders of magnitude in corrosion current density. Furthermore,

the anodic region of the Ti-bearing steel shows a narrow active-passive region (Fig. 3 inset), which is in contrast to the Ti-free steel. This small passive region may be ascribed to the formation of a relatively dense corrosion layer. Then as the potential increases, the current increases, which is likely due to the destruction of the corrosion layer. The cathodic curves of the polarization curves also shifted towards lower current densities in the presence of Ti.
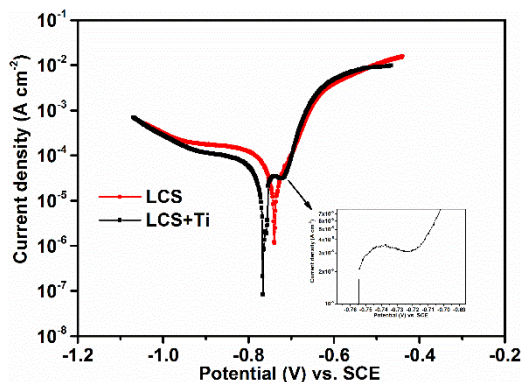
Fig. 3. PDP plot recorded after 24 hours of immersion at OCP in 3.5 wt.% NaCl saturated with CO_2

Table 3.
PDP parameters

Sample	E (V)	J_{corr} (μA cm^{-2})	CR(mm y^{-1})
LCS	-0.739	121.96	1.48
LCS+Ti	-0.765	72.24	0.87

The corrosion process in the presence of CO_2 is controlled by the cathodic (Eq. 5-7) and the anodic reactions (Eq. 8) [9, 24]:

$$2H_2CO_3 + 2e^- \rightarrow H_2 + 2HCO_3^- \tag{5}$$

$$2HCO_3^- + 2e^- \rightarrow H_2 + 2CO_3^{2-} \tag{6}$$

$$2H^+ + 2e^- \rightarrow H_2 \tag{7}$$

$$Fe \rightarrow Fe^{2+} + 2e^- \tag{8}$$

The pH of the tested solution is 4.3. At pH>4, the main cathodic reactions are reactions 5 and 6. The active domain referred to the metal dissolution (Eq. 8) [16]. The change in the shape observed is likely attributed to the formation of a thin passive protective surface film on the metal surface due to the presence of Ti, in agreement with the literature [12, 23, 25]. The results suggest that the addition of titanium hindered both the rate of the anodic dissolution (Eq. 8) and the cathodic reactions (Eq. 5-6), by either covering part of the metal surface and/or blocking the active corrosion sites on the steel surface. The efficiency calculated with the Eq. (2) shows an improvement of around 40%, which is consistent with the result of EIS.

3.3. Surface analysis

In a CO_2-containing solution, carbon dioxide dissolves to form H_2CO_3, which it dissociates in HCO_3^- and in CO_3^{2-}, according to the following reactions [26]:

$$CO_2 + H_2O \leftrightarrow H_2CO_3 \tag{9}$$

$$H_2CO_3 \leftrightarrow H^+ + HCO_3^- \tag{10}$$

$$HCO_3^- \leftrightarrow H^+ + CO_3^{2-} \tag{11}$$

If the concentrations of Fe^{2+} and CO_3^{2-} ions exceed the solubility limit, $FeCO_3$ precipitates on the surface [27-28]. However, no traces of $FeCO_3$ were found, but the Raman results reported in Fig. 4 and Table 4 show that the corrosion products observed were mainly composed of magnetite (Fe_3O_4) and α-Fe_2O_3 or/and γ-Fe_2O_3 [29-31].
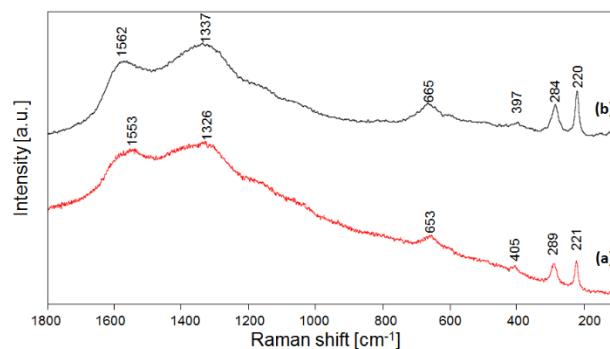
Fig. 4. Raman spectroscopy recorded after 24 hours of immersion after PDP experiment. (a) LCS; (b) LCS+Ti

Table 4.
Raman peaks and main compounds

Corrosion product	LCS wavenumber (cm^{-1})	LCS+Ti wavenumber (cm^{-1})
γ-Fe_2O_3	1563	1553
α-Fe_2O_3 γ-Fe_2O_3	1326	1337
α-Fe_2O_3 γ-Fe_2O_3 FeO	653	665
α-Fe_2O_3	405	397
α-Fe_2O_3	289	284
α-Fe_2O_3	221	220

The presence of these species is likely ascribed to the decomposition of $FeCO_3$, according to the following reaction [9, 27]:

$$FeCO_3 \rightarrow FeO + CO_2 \tag{12}$$

In turn, FeO transforms into Fe_3O_4 [9, 27].

$$3FeO + CO_2 \rightarrow Fe_3O_4 + CO \qquad (13)$$

$$3FeO + H_2O \rightarrow Fe_3O_4 + H_2 \qquad (14)$$

However, in the presence of oxygen, FeO and Fe_3O_4 transform into Fe_2O_3 [9, 27].

$$4FeO + O_2 \rightarrow 2Fe_2O_3 \qquad (15)$$

In the air: $4Fe_3O_4 + O_2 \rightarrow 6Fe_2O_3 \qquad (16)$
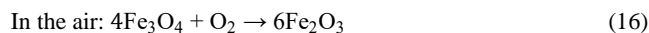
No traces of titanium oxide were observed, evidencing that the thickness of the passive TiO_2 layer was at a trace level below the detection limit of the instrument.

The SEM images of the steels after PDP experiments are shown in Fig. 5. The Ti-bearing steel showed a smoother surface compared with the Ti-free steel. The improvement may be attributed to the formation of a thin TiO_2 passive layer on the Ti-bearing surface resulting from the minor addition of Ti [25].
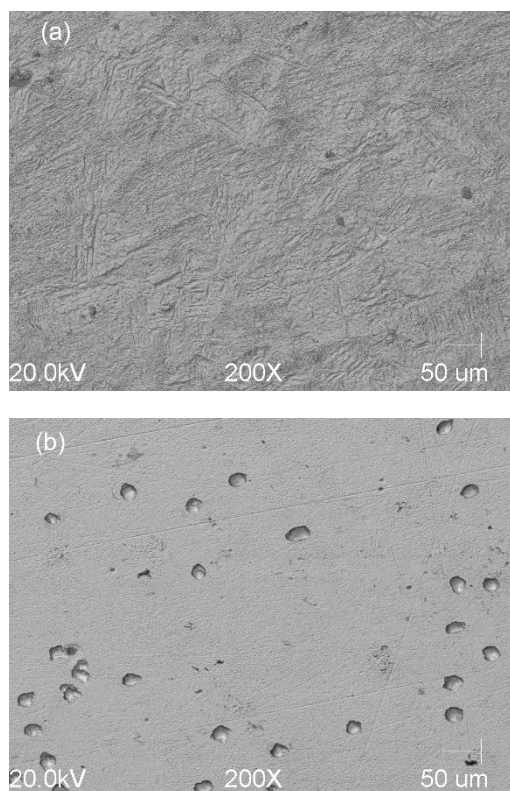
Fig. 5. SEM analysis of the steels after 24 hours of immersion in 3.5 wt.% NaCl saturated with CO_2. (a) LCS; (b) LCS+Ti.

4. Conclusions

The effect of microalloying with Ti on the corrosion behavior of low-carbon steels in a saline CO_2-containing environment can be summarized in the following points:

- The microstructure of Ti-bearing steel was finer compared to Ti-free steel.
- The EIS experiments showed that the addition of Ti improved the corrosion resistance of the LCS by around 30%. Moreover, the EIS experiment showed that the value of R_f (i.e., the polarisation resistance of the film) of the steel with Ti was higher than the Ti-free steel, indicating that Ti improved the corrosion resistance of the steel.
- The PDP results showed that microalloying with Ti, the corrosion current density decreased and a small passive region is observed.
- The corrosion products were mainly composed of different types of iron oxide.

Acknowledgments

References

[1] Yu, C., Wang, H., Gao, X. & Wang, H. (2020). Effect of Ti Microalloying on the Corrosion Behavior of Low-Carbon Steel in H2S/CO2 Environment. *Journal of Materials Engineering and Performance.* 29(9), 6118-6129. DOI:10.1007/s11665-020-05077-1.

[2] Liu, Z., Gao, X., Du, L., Li, J., Zheng, C. & Wang, X. (2018). Corrosion mechanism of low-alloy steel used for flexible pipe in vapor-saturated H2S/CO2 and H2S/CO2-saturated brine conditions. *Materials and Corrosion* 69(9), 1180-1195. DOI:10.1002/maco.201810047.

[3] Palumbo, G., Banaś, J., Bałkowiec, A., Mizera, J. & Lelek-Borkowska, U. (2014). Electrochemical study of the corrosion behaviour of carbon steel in fracturing fluid. *J. Solid State Electrochem.* 18(11), 2933-2945. DOI:10.1007/s10008-014-2430-2.

[4] Liu, Z.-G., Gao, X.-H., Du, L.-X., Li, J.-P., Li, P. & Misra, R.D.K. (2017). Comparison of corrosion behaviors of low-alloy steel exposed to vapor-saturated H2S/CO2 and H2S/CO2-saturated brine environments. *Materials and Corrosion* 68(5), 566-579. https://doi.org/10.1002/maco.201609165.

[5] Rozenfeld, I.L. (1981). *Corrosion Inhibitors*. New York: McGraw-Hill.

[6] Palumbo, G., Kollbek, K., Wirecka, R., Bernasik, A. & Górny, M. (2020). Effect of CO_2 partial pressure on the corrosion inhibition of N80 carbon steel by gum arabic in a CO_2-water saline environment for shale oil and gas industry. *Materials.* 13(19), 4245, 1-24. https://doi.org/10.3390/ma13194245.

[7] Bai, H., Wang, Y., Ma, Y., Zhang, Q., Zhang, N. (2018). Effect of CO2 partial pressure on the corrosion behavior of J55 carbon steel in 30% crude oil/brine mixture. *Materials.* 11(9), 1765, 1-15. DOI:10.3390/ma11091765.

[8] Cui, L., Kang, W., You, H., Cheng, J., & Li, Z. (2021). Experimental study on corrosion of J55 casing steel and N80

tubing steel in high pressure and high temperature solution containing CO2 and NaCl. *Journal of Bio- and Tribo-Corrosion.* 7(1), 13, 1-14. DOI:10.1007/s40735-020-00449-5.

[9] Islam, M.A., & Farhat, Z.N. (2015). Characterization of the corrosion layer on pipeline steel in sweet environment. *Journal of Materials Engineering and Performance.* 24(8), 3142-3158. DOI: 10.1007/s11665-015-1564-4.

[10] Zhang, T., Liu, W., Yin, Z., Dong, B., Zhao, Y., Fan, Y., Wu, J., Zhang, Z. & Li, X. (2020). Effects of the addition of Cu and Ni on the corrosion behavior of weathering steels in corrosive industrial environments. *Journal of Materials Engineering and Performance.* 29(4), 2531-2541. DOI: 10.1007/s11665-020-04738-5.

[11] Weng, L., Du, L. & Wu, H. (2018). Corrosion behaviour of weathering steel with high-content titanium exposed to simulated marine environment. *International Journal of Electrochemical Science.* 13(6), 5888-5903. DOI: 10.20964/2018.06.61.

[12] Marcus, P. (1994). On some fundamental factors in the effect of alloying elements on passivation of alloys. *Corrosion Science.* 36(12), 2155-2158. https://doi.org/10.1016/0010-938X(94)90013-2.

[13] Liu, Z., Gao, X., Du, L., Li, J., Li, P. (2016). Corrosion Behaviour of Low-Alloy Steel with Titanium Addition Exposed to Seawater Environment. *International Journal Electrochemical Science.* 11(8), 6540-6551. DOI: 10.20964/2016.08.25.

[14] Banas, J., Lelek-Borkowska, U., Mazurkiewicz, B. & Solarski, W. (2007). Effect of CO_2 and H_2S on the composition and stability of passive film on iron alloys in geothermal water. *Electrochim. Acta* 52(18), 5704-5714. DOI: 10.1016/j.electacta.2007.01.086.

[15] Palumbo, G., Dunikowski, D., Wirecka, R., Mazur, T., Lelek-Borkowska, U., Wawer, K. & Banaś, J. (2021). Effect of Grain Size on the Corrosion Behavior of Fe-3wt.%Si-1wt.%Al Electrical Steels in Pure Water Saturated with CO_2. *Materials.* 14(17), 5084, 1-19. https://doi.org/10.3390/ma14175084.

[16] Święch, D., Palumbo, G., Piergies, N., Pięta, E., Szkudlarek, A. & Paluszkiewicz, C. (2021). Spectroscopic investigations of 316L stainless steel under simulated inflammatory conditions for implant applications: the effect of tryptophan as corrosion inhibitor/hydrophobicity marker. *Coatings.* 11(9), 1097. https://doi.org/10.3390/coatings11091097.

[17] Święch, D., Paluszkiewicz, C., Piergies, N., Pięta, E., Kollbek, K. & Kwiatek, W.M. (2020). Micro- and nanoscale spectroscopic investigations of threonine influence on the corrosion process of the modified Fe surface by Cu nanoparticles. *Materials.* 13(20), 4482, 1-16. https://doi.org/10.3390/ma13204482.

[18] Chen, Z. & Yan, K. (2020). Grain refinement of commercially pure aluminum with addition of Ti and Zr elements based on crystallography orientation. *Scientific Reports.* 10(1), 16591, 1-8. https://doi.org/10.1038/s41598-020-73799-2.

[19] Kalisz, D. & Żak, P.L. (2015). Modeling of solute segregation and the formation of non-metallic inclusions during solidification of a titanium-containing steel. *Kovove Materialy.* 53(1), 35-41. DOI:10.4149/km_2015_1_35.

[20] Podorska, D., Drozdz, P., Falkus, J. & Wypartowicz, J. (2006). Calculations of oxide inclusions composition in the steel deoxidized with Mn, Si and Ti. *Archives of Metallurgy and Materials.* 51(4), 581-586. ISSN: 1733-3490.

[21] Zhang, M., Li, M., Wang, S., Chi, J., Ren, L., Fang, M. & Zhou, C. (2020). Enhanced wear resistance and new insight into microstructure evolution of in-situ (Ti,Nb)C reinforced 316 L stainless steel matrix prepared via laser cladding. *Optics and Lasers in Engineering.* 128, 106043, 1-10. DOI:10.1016/j.optlaseng.2020.106043.

[22] Sadeghpour, S., Kermanpur, A. & Najafizadeh, A. (2013). Influence of Ti microalloying on the formation of nanocrystalline structure in the 201L austenitic stainless steel during martensite thermomechanical treatment. *Materials Science and Engineering: A.* 584, 177-183. DOI:10.1016/j.msea.2013.07.014.

[23] Zhang, L.M., Ma, A.L., Hu, H.X.; Zheng, Y.G., Yang, B.J. & Wang, J.Q. (2017). Effect of microalloying with Ti or Cr on the corrosion behavior of Al-Ni-Y amorphous alloys. *Corrosion.* 74(1), 66-74. https://doi.org/10.5006/2451.

[24] Mustafa, A.H., Ari-Wahjoedi, B. & Ismail, M.C. (2013). Inhibition of CO2 corrosion of X52 steel by imidazoline-based inhibitor in high pressure CO2-water environment. *Journal of Materials Engineering and Performance.* 22(6), 1748-1755. DOI: 10.1007/s11665-012-0443-5.

[25] Nie, X.P., Yang, X.H. & Jiang, J.Z. (2009) Ti microalloying effect on corrosion resistance and thermal stability of CuZr-based bulk metallic glasses. *Journal of Alloys Compounds.* 481(1), 498-502. DOI: 10.1016/j.jallcom.2009.03.022.

[26] Palumbo, G., Górny, M. & Banaś, J. (2019). Corrosion inhibition of pipeline carbon steel (N80) in CO2-saturated chloride (0.5 M of KCl) solution using gum arabic as a possible environmentally friendly corrosion inhibitor for shale gas industry. *Journal of Materials Engineering and Performance.* 28(10), 6458-6470. https://doi.org/10.1007/s11665-019-04379-3.

[27] Heuer, J.K. & Stubbins, J.F. (1999). An XPS characterization of FeCO3 films from CO2 corrosion. *Corros. Sci.* 41(7), 1231-1243. https://doi.org/10.1016/S0010-938X(98)00180-2.

[28] Mora-Mendoza, J.L., Turgoose, S. (2002) Fe3C influence on the corrosion rate of mild steel in aqueous CO_2 systems under turbulent flow conditions. *Corrosion Science.* 44(6), 1223-1246. DOI:10.1016/S0010-938X(01)00141-X.

[29] Criado, M., Martínez-Ramirez, S. & Bastidas, J.M. (2015). A Raman spectroscopy study of steel corrosion products in activated fly ash mortar containing chlorides. *Construction and Building Materials.* 96, 383-390. http://dx.doi.org/10.1016/j.conbuildmat.2015.08.034.

[30] Zhang, X., Xiao, K., Dong, C., Wu, J., Li, X. & Huang, Y. (2011). In situ Raman spectroscopy study of corrosion products on the surface of carbon steel in solution containing Cl− and SO42. *Engineering Failure Analysis.* 18(8), 1981-1989. DOI:10.1016/j.engfailanal.2011.03.007.

[31] Święch, D., Paluszkiewicz, C., Piergies, N., Lelek-Borkowska, U. & Kwiatek, W.M. (2018). Identification of corrosion products on Fe and Cu metals using spectroscopic methods. *Acta Physica Polonica Series A.* 133(4), 286-288. DOI: 10.12693/APhysPolA.133.286.